Dalton Transactions

RSC Publishing

PAPER

View Article Online
View Journal | View Issue

Cite this: *Dalton Trans.*, 2013, **42**, 9914

Synthesis, characterization and bioimaging of fluorescent labeled polyoxometalates†

Georg Geisberger,[a] Emina Besic Gyenge,[b] Doris Hinger,[b] Peter Bösiger,[a] Caroline Maake[b] and Greta R. Patzke*[a]

Received 13th February 2013,
Accepted 3rd May 2013

DOI: 10.1039/c3dt50414j

www.rsc.org/dalton

A fluorescent labeled Wells–Dawson type POM ({$P_2W_{17}O_{61}$Fluo}) was newly synthesized and characterized by a wide range of analytical methods. {$P_2W_{17}O_{61}$Fluo} was functionalized with fluorescein amine through a stable amide bond, and its long time stability was verified by UV/vis spectroscopic techniques at physiologically relevant pH values. No significant impact on the cell viability or morphology of HeLa cells was observed for POM concentrations up to 100 μg mL^{-1}. Cellular uptake of fluorescent {$P_2W_{17}O_{61}$Fluo} was monitored by confocal laser scanning microscopy. POM uptake occurs mainly after prolonged incubation times of 24 h resulting in different intracellular patterns, *i.e.* randomly distributed over the entire cytoplasm, or aggregated in larger clusters. This direct monitoring strategy for the interaction of POMs with cells opens up new pathways for elucidating their unknown mode of action on the way to POM-based drug development.

Introduction

Polyoxometalates (POMs) have been attracting interdisciplinary research interest for decades due to their virtually unlimited structural flexibility which provides access to a wide range of key material properties.[1–5] The high bioactive potential of POMs has been under intense investigation since the 1980s, and their observed antibacterial, anticancer and antiviral activity opens up new perspectives for the development of low-cost and tuneable inorganic drugs, *e.g.* against new viral threats and the increasing problem of bacterial resistances.[6–11]

However, the multitude of empirical bioactivity data derived from POM-based *in vitro* and *in vivo* studies[12] did not afford a proportional degree of insight into their biochemical pathways. Localization of POMs in cells and clarification of their metabolization after endocytosis would provide essential information for understanding their modes of action. Tracking of POMs in cellular environments is furthermore indispensable to control their adverse effects, such as cytotoxicity, and to circumvent instability under physiological conditions. Over the past few years, an increasing number of drug delivery approaches for POM encapsulation has been developed, such as efficient anticancer POM–liposome composites.[13–16] Nevertheless, informed development of POM-based drug prototypes is delayed by a lack of direct visualization techniques.

Our recent studies were thus focused on nanocapsules based on bioactive POMs and various chitosan derivatives, preferably carboxymethyl chitosan (CMC) and trimethyl chitosan (TMC). These nanocomposites combine stability under ambient conditions with significantly lowered POM cytotoxicity.[17,18] Next, we demonstrated that POM–CMC composites can be safely shuttled into cancer cells. For the first time, we directly observed cellular uptake of bioactive POM composites: complementary CLSM (confocal laser scanning microscopy) and TEM (transmission electron microscopy) techniques on labeled and unlabeled nanocomposites, respectively, revealed that they are taken up within less than 1 h with a strong preference for the perinuclear region of HeLa cells.[19] As the next step towards elucidation of biochemical POM routes, we here present new evidence for cellular uptake of pristine POMs.

Microscopic tracking of fluorescent POMs containing lanthanoid heteroatoms, such as europium or gadolinium, appears to be the most straightforward approach at first glance. Unfortunately, it cannot be directly applied in biological media, because the luminescence of Ln-containing POMs can only be monitored in the solid state, whereas it is quenched in aqueous solutions by hydrate layers.[20,21] This renders attachment of a fluorescent dye to bioactive POMs a very promising strategy. However, derivatization of POMs with

[a]*Institute of Inorganic Chemistry, University of Zurich, Winterthurerstrasse 190, CH-8057 Zurich, Switzerland. E-mail: greta.patzke@aci.uzh.ch; Fax: (+) 41 44 635 6802*

[b]*Institute of Anatomy, University of Zurich, Winterthurerstrasse 190, CH-8057 Zurich, Switzerland*

†Electronic supplementary information (ESI) available: ^{31}P NMR spectra of {$P_2W_{17}O_{61}$Fluo} (Fig. S1), ^{1}H and ^{13}C NMR spectra of {$P_2W_{17}O_{61}$Fluo} (Fig. S2 and S3), UV/vis spectra of {$P_2W_{17}O_{61}$Fluo} (Fig. S4), FT-IT spectra of {$P_2W_{17}O_{61}$Fluo} after thermal treatment (Fig. S5), 3D CLSM images of HeLa cells (Fig. S6), CLSM image of control cells (Fig. S7), confocal pictures of HeLa cells after 1 h and 5 h of POM incubation (Fig. S8). See DOI: 10.1039/c3dt50414j

organic residues remains a challenge, and only a few approaches hitherto have been established to connect POM moieties with fluorescent dyes.[22–24] Moreover, the instability of many POMs at physiological pH severely limits the number of suitable candidates for such labeling reactions.

Viable routes towards stable organic functionalization of POMs have been published by Bareyt *et al.* and Carraro *et al*.[25,26] The first approach introduces POMs equipped with Sn-organyl derivatives carrying a carboxyl group, and the latter study modifies POMs with Si-organyls containing amino groups. Tin-functionalized POMs have furthermore been evaluated for their inhibitory potential against protein kinase CK2.[27] Here, we employ the Sn-organyl route *via* carboxyl-functionalized POMs for coupling reactions with fluorescein through amide bond formation.[28,29] The target POM $TBA_6K[\alpha_2\text{-}P_2W_{17}O_{61}\{Sn(CH_2)_2CONHC_{20}H_{11}O_5\}]$ contains the lacunary $[\alpha_2\text{-}P_2W_{17}O_{61}]^{10-}$ derivative of the Wells–Dawson polyanion $[P_2W_{18}O_{62}]^{6-}$, which is a prototype bioactive POM. It excels through antibacterial activity against resistant strains and has been widely investigated and derivatized as an anti-HIV agent.[30–32] Insulin mimetic[33] and neurite outgrowth effects[34] furthermore amplify the bio-medical spectrum of Wells–Dawson-type POMs. Concerning their lacunary derivatives, interaction of $[P_2W_{17}O_{61}]^{10-}$ with human serum albumin (HSA) has been studied.[35] Zr-substituted derivatives have recently been identified as selective catalysts for peptide bond hydrolysis,[36] while gadolinium introduction opens up new possibilities for MRI contrast agents.[37,38]

In the following, we present the synthesis and characterization of fluorescent labeled Wells–Dawson POMs, followed by direct monitoring of their interaction with cancer cells.

Results and discussion

Synthesis of fluorescein labeled POMs

Our route towards fluorescent labeled POMs started from the pioneering approach of Bareyt *et al.* for the versatile functionalization of the lacunary Wells–Dawson heteropolyanion $K_{10}[\alpha_2\text{-}P_2W_{17}O_{61}]$ *via* a tin organyl moiety equipped with a reactive carboxyl group.[25] As this carboxyl "anchor" can be easily modified into esters or amides, we labeled the POM with fluorescein through amide bond formation. EEDQ was employed as a coupling agent to combine fluorescein amine and the derivatized POM into $TBA_6K[\alpha_2\text{-}P_2W_{17}O_{61}\{Sn(CH_2)_2\text{-}CONHC_{20}H_{11}O_5\}]$ (labeled POM henceforth abbreviated as $\{P_2W_{17}O_{61}Fluo\}$, *cf.* Fig. 1).

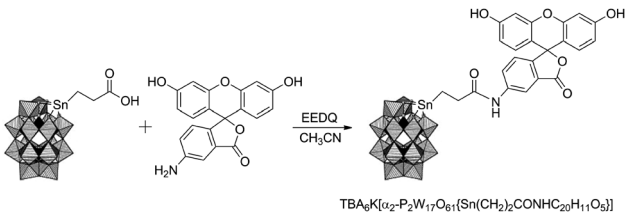

Fig. 1 Synthesis of $TBA_6K[\alpha_2\text{-}P_2W_{17}O_{61}\{Sn(CH_2)_2CONHC_{20}H_{11}O_5\}]$ labeled with fluorescein amine.

Characterization of fluorescein labeled POMs

Structure and stability. Thermogravimetric analysis of $\{P_2W_{17}O_{61}Fluo\}$ showed that the fluorescent labeled POM contains 10 aqua ligands and remains stable up to 300 °C, followed by decomposition of the organic moiety at higher temperatures. Elemental analysis of $\{P_2W_{17}O_{61}Fluo\}$ provides strong evidence for successful fluorescein coupling with negligible differences between analytical and calculated C and H contents and a slight deviation (around 0.4) for N. Reaction progress was furthermore monitored *via* ^{31}P NMR (Fig. S1†). The structural integrity of the precursors and the final compound was verified by NMR spectroscopy (Fig. S2 and S3†).

Stability of $\{P_2W_{17}O_{61}Fluo\}$ was investigated under conditions as close as possible to cell culture media (PBS, pH 7.2). Analogous to cellular uptake experiments, the labeled POM was first dissolved in DMSO to yield a 0.3% (v/v) DMSO in PBS solution after combination of both media. Interestingly, $\{P_2W_{17}O_{61}Fluo\}$ did not precipitate upon PBS addition, thus eliminating the need for subsequent ion exchange reactions prior to cellular uptake tests.

The solubility of TBA-$\{P_2W_{17}O_{61}Fluo\}$ in aqueous media strongly depends on their components in combination with the pH value: dissolution was observed in PBS or cell culture medium (DMEM) at pH values above 7, whereas precipitation sets in at lower pH values or in water.

The UV/vis spectrum of $\{P_2W_{17}O_{61}Fluo\}$ in PBS (Fig. 2) clearly indicates its stability around neutral pH conditions through monitoring of the characteristic POM absorption bands, *i.e.* two charge-transfer shoulders (O → W) at 257 and 289 nm and a fluorescein-based absorption with a maximum at 458 nm (Fig. 2b) which overlaps with POM bands in the UV region. These characteristic POM absorption bands did not undergo significant changes at any wavelength over a period of 5 days (Fig. S4†). These results agree well with the previously observed stability of a representative Sn-substituted Wells–Dawson type POM in physiological media.[25]

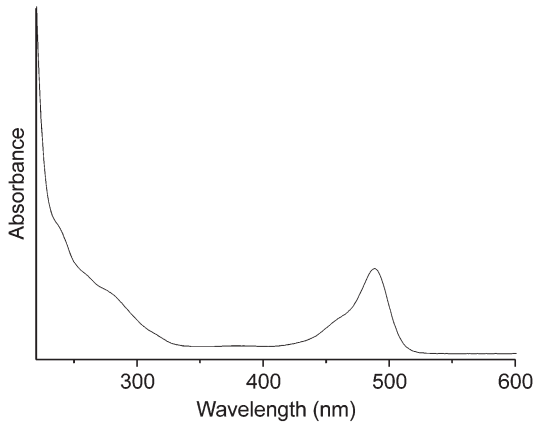

Fig. 2 UV/vis spectrum of $\{P_2W_{17}O_{61}Fluo\}$ in PBS.

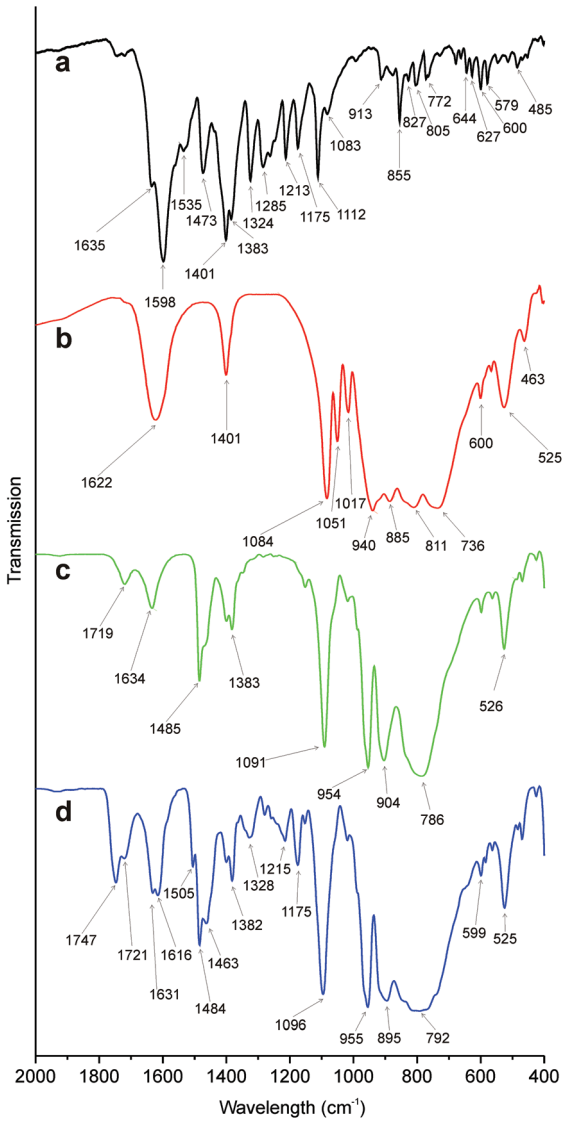

Fig. 3 FT-IR spectra of (a) fluorescein amine, (b) $\{P_2W_{17}O_{61}\}$, (c) $\{P_2W_{17}O_{61}Sn\}$ and (d) $\{P_2W_{17}O_{61}Fluo\}$.

FT-IR spectroscopy. FT-IR spectra of fluorescein amine, $K_{10}[\alpha_2\text{-}P_2W_{17}O_{61}]$ ($\{P_2W_{17}O_{61}\}$), $TBA_6K[\alpha_2\text{-}P_2W_{17}O_{61}\{Sn(CH_2)_2\text{-}COOH\}]$ ($\{P_2W_{17}O_{61}Sn\}$) and $\{P_2W_{17}O_{61}Fluo\}$ are compared in Fig. 3. Functionalization with the tin organyl moiety affects the band positions of the POM scaffold (Fig. 3b and c), and two new bands appear at 1719 and 1485 cm^{-1} which can be attributed to the carboxyl group and the vibrations of the organic side chain. Key vibrations of $TBA_6K[\alpha_2\text{-}P_2W_{17}O_{61}\{Sn(CH_2)_2\text{-}COOH\}]$ are summarized in Table S1,† and the characteristic bands of the aryl moiety (*e.g.* at 1400, 1382, 1327, 1280, 1256, 1242, 1215 and 1175 cm^{-1}) illustrate the successful coupling of POM and fluorescein amine. The labeled POM withstands heating to 200 °C as can be seen from FT-IR spectra (Fig. S5†).

***In vitro* cell viability tests.** Fluorescein labeled POMs (50 and 100 μg mL^{-1}) were tested for cytotoxicity *vs.* HeLa cells with cell viability (MTT) assays (Fig. 4). Cells incubated under conditions described in the Experimental section (below) did not display significant viability changes in comparison with controls grown in cell culture media. Experiments with the water-soluble sodium salt of $\{P_2W_{17}O_{61}Fluo\}$ and with TBA-$\{P_2W_{17}O_{61}Fluo\}$ led to comparable results. All in all, no significant toxicity of $\{P_2W_{17}O_{61}Fluo\}$ towards HeLa cells could be detected.

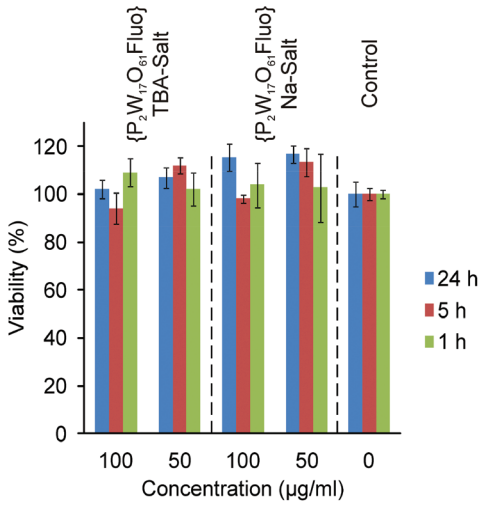

Fig. 4 MTT assays of TBA- and Na-$\{P_2W_{17}O_{61}Fluo\}$.

Cellular uptake of fluorescent POMs

Cellular uptake tests were performed on HeLa cells which were incubated with 50 and 100 μg mL^{-1} TBA-$\{P_2W_{17}O_{61}Fluo\}$ and Na-$\{P_2W_{17}O_{61}Fluo\}$, respectively, for 1, 5 and 24 h (for details *cf.* Experimental section). Both TBA- and Na-$\{P_2W_{17}O_{61}Fluo\}$ display related time-dependent uptake kinetics: only very few particles are visible in the cells after 1 h and 5 h of incubation (Fig. S8†), but prolonged treatment (24 h) led to uptake of larger POM quantities (Fig. 5). Compared to our preceding cellular uptake studies on fluorescent labeled POM nanocomposites, pristine POMs display similar uptake behavior, albeit with a slight delay.[18,19]

POM uptake was monitored by CLSM on HeLa cells, and Fig. 5 shows the cells after 24 h of incubation with fluorescent $\{P_2W_{17}O_{61}Fluo\}$.

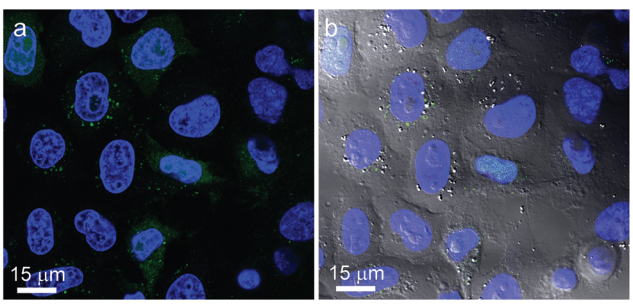

Fig. 5 (a) Confocal picture of HeLa cells with stained nucleus (blue) incubated with 50 μg mL^{-1} TBA-$\{P_2W_{17}O_{61}Fluo\}$ (green) for 24 h; (b) confocal picture merged with the DIC image showing the intact cell morphology.

POM localization exhibits two different patterns, namely random distribution or formation of large clusters in the cell cytoplasm. It is currently not clear whether this is the result of *e.g.* alternative internalization modes or intracellular processing pathways. Colocalization with mitochondria was not observed, but cluster accumulation might occur in trafficking or recycling vesicles. However, distributions of $\{P_2W_{17}O_{61}Fluo\}$ signals were notably different from those found in our previous study with fluorescent labeled POM nanocomposites that featured mainly perinuclear localization.[19] Given that TBA- and Na-salts of $\{P_2W_{17}O_{61}Fluo\}$ did not differ significantly with respect to cellular uptake, the countercation does not appear to play a crucial role in the process.

Location of $\{P_2W_{17}O_{61}Fluo\}$ within HeLa cells after 24 h of incubation was furthermore verified by z-stack recordings. Section views focusing on a selected POM cluster located in all planes are shown in Fig. S6a, and Fig. S6b† provides a 3D maximum projection visualizing the amounts and cluster shapes of POMs within cells. Note that strong and homogeneous POM uptake is not equally displayed by all cells. This may be due to active POM uptake and might thus reflect inhomogeneous activity of the cell population, but further investigations using immunocytochemistry methods are required to track endocytotic pathways.

Fluorescent labeled POMs were never found to enter the nucleus, regardless of concentration or incubation time. This key observation does not support any active interaction of POMs with nuclear DNA and their role as possible mutagens under the given conditions. This also sheds new light on the antiviral properties and additional bio-medical effects of Dawson-type POMs which are probably proceeding without direct POM–DNA interactions.[31]

Earlier, Cibert and Jasmin employed different spectroscopic methods to demonstrate that ammonium-21-tungsto-9-antimonate (HPA-23) is capable of entering C3HBi fibroblasts.[39] The authors furthermore concluded from these indirect observations that POMs enter cells, but do not aggregate in any cell organelles. Our results newly reveal the presence of large POM aggregates inside cells. While we can only exclude their colocalization with mitochondria on the basis of our study, nothing is currently known with respect to other organelles. However, it may be speculated that POMs (dispersed or in clusters) are encapsulated within membrane-bound vesicles, as reported for silica nanoparticles by Besic Gyenge *et al.*[40]

As expected from MTT assays, differential interference contrast (DIC) images (Fig. 5b) demonstrate intact cell morphologies after POM uptake in line with control samples (Fig. S7†). However, one noteworthy difference is evident: cells containing large POM aggregates generally displayed more vacuoles than those without such POM clusters or control cells. However, confocal images also show that these vacuoles do not contain POMs. Their frequent formation may indicate a certain extent of stress on the cells. Whereas our microscopic observations correspond with preceding reports on vacuole appearance in POM-treated cells by Boudinot *et al.*,[41] we could not confirm their hypothesis of POM location within such vacuoles.

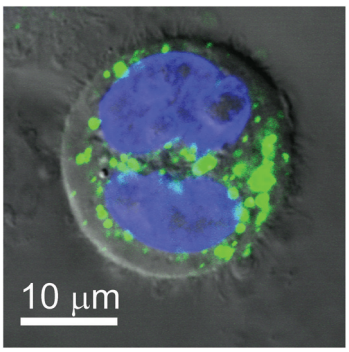

Fig. 6 Confocal picture merged with the DIC image of a HeLa cell during cleavage incubated with 50 μg mL^{-1} TBA-$\{P_2W_{17}O_{61}Fluo\}$ (green; nucleus: blue) for 24 h.

We furthermore observed POM-containing HeLa cells during telophase in the late stages of cell cleavage (Fig. 6). Labeled POM aggregates are found over the entire cell cytoplasm and they are equally distributed between the two emerging daughter cells. This points to a certain persistence of POMs within the cellular environment, wherein they are rather accumulated and redistributed than quickly degraded.

Furthermore, POM uptake by HeLa cells was verified by ICP-MS analysis on lyophilized samples (Table 1), and protein contents were determined in parallel (for details *cf.* Experimental below). Control experiments with or without fluorescein amine in the absence of POMs did not display any tungsten above the analytical detection limits, *i.e.* background concentrations in cells can be excluded. After treatment with $\{P_2W_{17}O_{61}Fluo\}$, however, tungsten contents of HeLa cells sharply raised to *ca.* 3.28 μg mg^{-1} protein or 0.98 pg per cell, respectively. Interestingly, comparable tungsten amounts were found after treatment of HeLa cells with unlabeled POM ($K_6[P_2W_{18}O_{62}]\cdot 16H_2O$) (2.70 μg mg^{-1} protein corresponding to 0.81 pg W per cell). These results indicate that fluorescein amine-labeling does not substantially influence the POM uptake process. Most importantly, the cellular uptake of tungsten species provides strong evidence that the observed fluorescence signals (Fig. 5 and 6) indeed arise from intact $\{P_2W_{17}O_{61}Fluo\}$, given that its stability in neutral media is evident from spectroscopic data (Fig. 2 and S4†).

Table 1 Tungsten contents in HeLa cells incubated for 24 h with 100 μg mL^{-1} TBA-$\{P_2W_{17}O_{61}Fluo\}$ (POM-Fluo), unlabeled POM ($K_6[P_2W_{18}O_{62}]\cdot 16H_2O$) or fluorescein amine (equalized to the labeled POM sample)

	Total protein [mg]	W [μg mg^{-1} protein]	W [pg per cell[b]]	POM [pg per cell]
Untreated control	4.12	0.00[a]	0.00[a]	0.00[a]
POM	3.88	2.70	0.81	1.07
POM-Fluo	3.12	3.28	0.98	1.31
Fluorescein amine	4.02	0.00[a]	0.00[a]	0.00[a]

[a] 0 or below detection limit. [b] Total protein content of HeLa cells was assumed to be 300 pg per cell.[42]

To the best of our knowledge, cellular uptake of POMs has never been determined before with comparable accuracy. Reference data for cellular contents of physiologically less abundant transition metal ions are generally rather rare. Nevertheless, we compared the above results to different metal uptake scenarios, starting with gallium uptake by HL 60 cells as a representative example of a non-essential metal ion.[43] Here, considerably lower cellular metal contents of 3.5×10^{-4} pg Ga per cell in comparison with the above tungsten concentrations were observed. Next, we found our tungsten contents to be in the same range as platinum contents in HeLa cells after treatment with cisplatin (1.12 ± 0.07 μg Pt mg^{-1} protein)[44] which indicates that POM levels in HeLa cells might be of interest for further studies. Finally, HeLa cells treated with magnetodendrimers for magnetic resonance tracking contained much more iron (13.6 ± 5.5 pg iron per cell) compared to POM uptake.[45]

Conclusions

New fluorescent labeled Wells–Dawson POMs were obtained through connection of functionalized lacunary POMs with fluorescein *via* amide linkage. Specifically, $K_{10}[\alpha_2\text{-}P_2W_{17}O_{61}]$ was equipped with a carboxy-functionalized tin organyl which subsequently formed a stable amide bond with fluorescein. Fluorescent labeling of $TBA_6K[\alpha_2\text{-}P_2W_{17}O_{61}\{Sn(CH_2)_2\text{-}CONHC_{20}H_{11}O_5\}]$ was verified with a wide arsenal of analytical methods including elemental analysis, FT-IR, NMR, and UV/vis spectroscopy. $\{P_2W_{17}O_{61}Fluo\}$ is soluble in PBS and cell culture medium (DMEM) at physiologically relevant pH values. Stability of $\{P_2W_{17}O_{61}Fluo\}$ over several days under cell test conditions was established by UV/vis spectroscopy. No cytotoxicity of $\{P_2W_{17}O_{61}Fluo\}$ towards HeLa cells was observed for concentrations up to 100 μg mL^{-1} regardless of the POM countercation, and cell viability as well as morphology were not significantly changed.

Cellular uptake tests furthermore provided the first evidence of localization of pristine POMs within cells, and two different intracellular distribution patterns were observed. Fluorescent POMs may either appear as randomly dispersed signals over the entire cytoplasm, or aggregated in clusters, which may point towards an organelle-related localization site. Importantly, we found no evidence for POMs entering the nucleus for various concentrations and incubation times, which calls for new in-depth investigations into their empirically observed antiviral and anticancer activity. Tungsten concentrations in HeLa cells are around 0.98 and 0.81 pg W per cell after treatment with labeled and pristine POMs, respectively. Consequently, FITC-labeling does not strongly influence the POM uptake process. The POM contents appear to be in a promising range for further bioactivity studies which are currently underway.

All in all, we introduce new fluorescent labeled POMs as important monitoring agents to directly track their biomedical modes of action. This approach opens up innovative perspectives to tailor low-cost POM drugs through unprecedented insight into their biochemical interactions and pathways.

Experimental

Materials

All used reagents were purchased from Sigma-Aldrich or Acros as ACS reagents and used as received.

Synthesis of $TBA_6K[\alpha_2\text{-}P_2W_{17}O_{61}\{Sn(CH_2)_2CONHC_{20}H_{11}O_5\}]$

EEDQ (19.2 mg, 0.08 mmol, 1.5 eq.) was dissolved in acetonitrile (5.5 mL) under reflux (80 °C) in a N_2 atmosphere. $TBA_6K[\alpha_2\text{-}P_2W_{17}O_{61}\{Sn(CH_2)_2COOH\}]$ (0.30 g, 0.05 mmol) was added and the mixture was stirred for 15 min. Afterwards, fluorescein amine (53.7 mg, 0.16 mmol) was added and the solution was refluxed at 90 °C for 24 h whereupon the color changed from yellow to orange. Reaction progress was monitored by ^{31}P-NMR. After completion of the reaction, the solvent was removed under vacuum and the orange oily residue was taken up in a minimum of acetonitrile. The product was precipitated through THF addition and collected by filtration. After several washing steps with THF the product was dried *in vacuo*. Yield: 218 mg (0.03 mmol, 69%, orange solid).

FT-IR (KBr): ν = 3458 (m), 3368 (m), 3213 (m), 2962 (s), 2935 (s), 2873 (s), 1747 (m), 1721 (w), 1631 (m), 1616 (m), 1505 (w), 1484 (m), 1463 (m), 1400 (w), 1382 (w), 1327 (w), 1280 (w), 1256 (w), 1242 (w), 1215 (w), 1175 (w), 1096 (s), 955 (s), 895 (s), 792 (s, br), 599 (w), 525 (m).

^{1}H NMR (400 MHz, CD_3CN): 0.99 (t, 84H, $^2J_{H-H}$ = 7.3, $N(CH_2CH_2CH_2CH_3)_4$), 1.28 (m, 2H, $SnCH_2$), 1.42 (m, 56H, $N(CH_2CH_2CH_2CH_3)_4$), 1.65 (m, 56H, $N(CH_2CH_2CH_2CH_3)_4$), 2.75 (m, 2H, CH_2CO), 3.16 (m, 56H, $N(CH_2CH_2CH_2CH_3)_4$), 6.57, 6.69, 6.88, 7.00, 7.07 (m, 9H, Ar-*H*), 7.22 (m, 1H, N*H*).

^{13}C NMR (100 MHz, CD_3CN): 2.0 ($SnCH_2$), 14.0 ($N(CH_2CH_2CH_2CH_3)_4$), 20.4 ($N(CH_2CH_2CH_2CH_3)_4$), 24.5 ($N(CH_2CH_2CH_2CH_3)_4$), 32.1 (CH_2CON), 59.4 ($N(CH_2CH_2CH_2CH_3)_4$), 68.3 (C_{quat}-fluorescein), 103.4, 108.0, 111.0, 112.8, 113.2, 118.3, 123.0, 125.3, 129.3 & 130.3 (CH-arom.), 150.9 & 153.4 (C_{quat}-arom.), 159.7 (*C*OO), 170.7 (CH_2CON).

^{31}P NMR (121.5 MHz, CD_3CN): −12.37 (s, 1P, PW_9), −10.27 (s, 1P, PW_8Sn).

Elemental analysis (%) calcd. for $C_{119}H_{224}KN_7O_{67}P_2W_{17}Sn$ (6170.10 g mol^{-1}):

C 23.16, H 3.66, N 1.59; found: C 22.52, H 3.60, N 1.12.

UV/vis (CH_3CN): 257 nm, 289 nm, 458 nm.

UV/vis (PBS): 238 nm, 259 nm, 280 nm, 457 nm, 489 nm.

Ion exchange

$Na_7[\alpha_2\text{-}P_2W_{17}O_{61}\{Sn(CH_2)_2CONHC_{20}H_{11}O_5\}]$. An exchange column (diameter 20 mm, length 400 mm) was 50% filled with a sodium-loaded Amberlite IR-120 cation exchanger.

$TBA_6K[\alpha_2\text{-}P_2W_{17}O_{61}\{Sn(CH_2)_2CONHC_{20}H_{11}O_5\}]$ (50 mg) was dissolved in CH_3CN (1 mL) under sonication and 0.5 mL water was added. The solution was dropped on the column and

slowly eluated by a mixture of CH_3CN–H_2O with increasing water content. The ratios of CH_3CN–H_2O were: 1 : 1, 1 : 2, 1 : 4, 1 : 6, 1 : 8, followed by pure H_2O. The solvent was removed under vacuum and the product was obtained as an orange solid.

Cell viability assay

HeLa cells were seeded onto 96-well plates (Corning) at a density of 3000 cells per well in DMEM + 10% FCS and kept overnight under standard conditions (37 °C, 5% CO_2, humidified atmosphere). The medium was replaced by DMEM containing $\{P_2W_{17}O_{61}Fluo\}$ as Na or TBA salt in different concentrations (50 and 100 μg mL^{-1}), and the cells were incubated for 1, 5 and 24 h. TBA-$\{P_2W_{17}O_{61}Fluo\}$ was first dissolved in a minimal amount of DMSO and then added to the growth media with a final concentration of 0.3% (v/v) of DMSO. After removal of the respective solutions, DMEM containing MTT (0.5 mg mL^{-1}) was added to the cells. MTT is converted by living cells after further incubation for 3 h. The metabolic product formazan was solubilized by replacing the MTT containing medium with dimethyl sulfoxide. After mixing, the absorption was recorded at 565 nm using a microplate luminometer (synergy2, BioTek). For each concentration and incubation time sextets were performed to determine the standard deviation. Results are expressed as means ± SD. Data were analyzed by one-way ANOVA with the *post hoc* Tukey's test applied for paired comparisons ($p < 0.05$; GraphPad Prism3).

Cellular uptake

HeLa cells were seeded either on 100 mm cell culture dishes or on PLL pretreated (0.25 mg mL^{-1} for 1 h, 37 °C) glass coverslides overnight. Na-$\{P_2W_{17}O_{61}Fluo\}$ was directly dissolved in the incubation medium. Experiments with TBA-$\{P_2W_{17}O_{61}Fluo\}$ were performed similar to MTT assays, *i.e.* at a final concentration of 0.3% (v/v) DMSO in DMEM after initial dissolution of the POM in a minimal volume of DMSO. Cells were incubated over several periods of time (1, 5 and 24 h) with 50 and 100 μg mL^{-1} TBA- and Na-$\{P_2W_{17}O_{61}Fluo\}$, respectively, diluted in a growth medium (DMEM supplemented with 10% FCS and 1% penicillin/streptomycin) in two concentrations (50 and 100 μg mL^{-1}) at 37 °C in a 5% CO_2 atmosphere. Hoechst (bisbenzimide H, 2 mM) was used for staining of nuclei. Visualization of mitochondria was performed with 200 nM MitoTracker® Orange CMTMRos. The individual dyes for CLSM studies were carefully selected to prevent overlapping of excitation and emission wavelengths. After incubation times of 30 min for both staining dyes at 37 °C, the cells were washed once with PBS and subsequently fixed with 1% paraformaldehyde for 15 min at room temperature. The slides were mounted with a Dako ImmunoMount medium and examined with a confocal laser scanning microscope SP2 (Leica, Germany).

For ICP-MS analysis the cells in 100 mm dishes were treated as described above for 24 h with 100 μg mL^{-1} of TBA-$\{P_2W_{17}O_{61}Fluo\}$, an equalized amount of unlabeled POM ($K_6[P_2W_{18}O_{62}]\cdot 16H_2O$) or an equalized amount of fluorescein amine, respectively. An untreated control was also included. The cells were detached with Trypsin (Sigma), extensively washed 3 times with PBS and subsequently lyophilized. Cellular uptake of tungsten, as the major element in POMs, was quantified in duplicates with ICP-MS techniques at Mikroanalytisches Labor Pascher (Remagen/Germany). In an aliquot of the sample the protein content was measured in parallel with the BCA protein assay kit from Pierce according to manufacturer's instructions. Overall POM uptake was calculated and normalized against the protein content of each sample.

Analytical characterization of the POMs

Fourier transform infrared (FT-IR) spectra were recorded on a Perkin-Elmer Spectrum Two™ using KBr pellets. UV/vis spectra were recorded on a PerkinElmer Lambda 650S UV/Vis spectrometer with a 10 mm cuvette. NMR spectroscopy was performed on a Bruker AV-2 400 spectrometer. All chemical shifts are expressed in parts per million (ppm) and referenced to the residual signals of the solvent.[46] In the case of $^{31}P\{^1H\}$ NMR spectra the chemical shifts are referenced to H_3PO_4 (85%) as an external standard. Elemental analysis of the title compound was carried out on an LECO CHNS-932 Elemental Analyzer on samples dried *in vacuo*.

Acknowledgements

This work was supported by the Swiss National Science Foundation (SNSF Professorship PP00P2_133483/1) and financial support from the University of Zurich is gratefully acknowledged. We thank the Center for Microscopy and Image Analysis, ZMB, University of Zurich, for support. The human cell line HeLa derived from cervical cancer was kindly provided by Prof. Peter Sonderegger (Department of Biochemistry, University of Zurich).

Notes and references

1 U. Kortz, A. Mueller, J. van Slageren, J. Schnack, N. S. Dalal and M. Dressel, *Coord. Chem. Rev.*, 2009, **253**, 2315.
2 D.-L. Long, E. Burkholder and L. Cronin, *Chem. Soc. Rev.*, 2007, **36**, 105.
3 H. N. Miras, G. J. T. Cooper, D.-L. Long, H. Boegge, A. Mueller, C. Streb and L. Cronin, *Science*, 2010, **327**, 72.
4 O. Oms, A. Dolbecq and P. Mialane, *Chem. Soc. Rev.*, 2012, **41**, 7497.
5 D. Drewes, E. M. Limanski and B. Krebs, *Dalton Trans.*, 2004, 2087.
6 B. Hasenknopf, *Front. Biosci.*, 2005, **10**, 275.
7 C. Schoeberl, R. Boehner, B. Krebs, C. Mueller and A. Barnekow, *Int. J. Oncol.*, 1998, **12**, 153.
8 J. T. Rhule, C. L. Hill and D. A. Judd, *Chem. Rev.*, 1998, **98**, 327.
9 A. Fluetsch, T. Schroeder, M. G. Gruetter and G. R. Patzke, *Bioorg. Med. Chem. Lett.*, 2011, **21**, 1162.

10 C. E. Mueller, J. Iqbal, Y. Baqi, H. Zimmermann, A. Roellich and H. Stephan, *Bioorg. Med. Chem. Lett.*, 2006, **16**, 5943.
11 H. U. V. Gerth, A. Rompel, B. Krebs, J. Boos and C. Lanvers-Kaminsky, *Anti-Cancer Drugs*, 2005, **16**, 101.
12 H. Stephan, M. Kubeil, F. Emmerling and C. E. Müller, *Eur. J. Inorg. Chem.*, 2013, 1585.
13 Y. Yang, J. H. He, X. H. Wang, B. Li and J. F. Liu, *Transition Met. Chem.*, 2004, **29**, 96.
14 X. H. Wang, F. Li, S. X. Liu and M. T. Pope, *J. Inorg. Biochem.*, 2005, **99**, 452.
15 T. Meissner, R. Bergmann, J. Oswald, K. Rode, H. Stephan, W. Richter, H. Zanker, W. Kraus, F. Emmerling and G. Reck, *Transition Met. Chem.*, 2006, **31**, 603.
16 H. El Moll, W. Zhu, E. Oldfield, L. M. Rodriguez-Albelo, P. Mialane, J. Marrot, N. Vila, I. M. Mbomekalle, E. Riviere, C. Duboc and A. Dolbecq, *Inorg. Chem.*, 2012, **51**, 7921.
17 G. Geisberger, S. Paulus, M. Carraro, M. Bonchio and G. R. Patzke, *Chem.–Eur. J.*, 2011, **17**, 4619.
18 G. Geisberger, E. B. Gyenge, C. Maake and G. R. Patzke, *Carbohydr. Polym.*, 2013, **91**, 58.
19 G. Geisberger, S. Paulus, E. B. Gyenge, C. Maake and G. R. Patzke, *Small*, 2011, **7**, 2808.
20 C. Zhang, R. C. Howell, Q. H. Luo, H. L. Fieselmann, L. J. Todaro and L. C. Francesconi, *Inorg. Chem.*, 2005, **44**, 3569.
21 M. T. Pope, in *Handbook on the Physics and Chemistry of Rare Earths*, ed. K. A. Gschneidner Jr., J.-C. G. Buenzli and V. K. Pecharsky, North Holland, Amsterdam, 2007, vol. 38, p. 337.
22 A. Dolbecq, E. Dumas, C. R. Mayer and P. Mialane, *Chem. Rev.*, 2010, **110**, 6009.
23 F. Odobel, M. Severac, Y. Pellegrin, E. Blart, C. Fosse, C. Cannizzo, C. R. Mayer, K. J. Eliott and A. Harriman, *Chem.–Eur. J.*, 2009, **15**, 3130.
24 A. Dolbecq, P. Mialane, F. Secheresse, B. Keita and L. Nadjo, *Chem. Commun.*, 2012, **48**, 8299.
25 S. Bareyt, S. Piligkos, B. Hasenknopf, P. Gouzerh, E. Lacote, S. Thorimbert and M. Malacria, *Angew. Chem., Int. Ed.*, 2003, **42**, 3404.
26 M. Carraro, G. Modugno, G. Fiorani, C. Maccato, A. Sartorel and M. Bonchio, *Eur. J. Org. Chem.*, 2012, 281.
27 R. Prudent, V. Moucadel, B. Laudet, C. Barette, L. Lafanechère, B. Hasenknopf, J. Li, S. Bareyt, E. Lacôte, S. Thorimbert, M. Malacria, P. Gouzerh and C. Cochet, *Chem. Biol.*, 2008, **15**, 683.
28 S. Bareyt, S. Piligkos, B. Hasenknopf, P. Gouzerh, E. Lacote, S. Thorimbert and M. Malacria, *J. Am. Chem. Soc.*, 2005, **127**, 6788.
29 K. Micoine, B. Hasenknopf, S. Thorimbert, E. Lacote and M. Malacria, *Org. Lett.*, 2007, **9**, 3981.
30 M. Inoue, T. Suzuki, Y. Fujita, M. Oda, N. Matsumoto and T. Yamase, *J. Inorg. Biochem.*, 2006, **100**, 1225.
31 Y. Inouye, Y. Fujimoto, M. Sugiyama, T. Yoshida and T. Yamase, *Biol. Pharm. Bull.*, 1995, **18**, 996.
32 D. A. Judd, J. H. Nettles, N. Nevins, J. P. Snyder, D. C. Liotta, J. Tang, J. Ermolieff, R. F. Schinazi and C. L. Hill, *J. Am. Chem. Soc.*, 2001, **123**, 886.
33 K. Nomiya, H. Torii, T. Hasegawa, Y. Nemoto, K. Nomura, K. Hashino, M. Uchida, Y. Kato, K. Shimizu and M. Oda, *J. Inorg. Biochem.*, 2001, **86**, 657.
34 M. Oda, M. Inoue, K. Hino, Y. Nakamura and T. Yamase, *Biol. Pharm. Bull.*, 2007, **30**, 787.
35 G. Zhang, B. Keita, C. T. Craescu, S. Miron, P. de Oliveira and L. Nadjo, *Biomacromolecules*, 2008, **9**, 812.
36 G. Absillis and T. N. Parac-Vogt, *Inorg. Chem.*, 2012, **51**, 9902.
37 G. Sun, J. Feng, H. Wu, F. Pei, K. Fang and H. Lei, *J. Magn. Magn. Mater.*, 2004, **281**, 405.
38 J. A. Barreto, W. O'Malley, M. Kubeil, B. Graham, H. Stephan and L. Spiccia, *Adv. Mater.*, 2011, **23**, H18.
39 C. Cibert and C. Jasmin, *Biochem. Biophys. Res. Commun.*, 1982, **108**, 1424.
40 E. B. Gyenge, X. Darphin, A. Wirth, U. Pieles, H. Walt, M. Bredell and C. Maake, *J. Nanobiotechnol.*, 2011, 9.
41 L. Ni, P. Greenspan, R. Gutman, C. Kelloes, M. A. Farmer and F. D. Boudinot, *Antiviral Res.*, 1996, **32**, 141.
42 H. Lodish, *et al*. *Molecular Cell Biology*, W. H. Freeman & Co, 3rd edn, 1995.
43 C. R. Chitambar and D. Sax, *Blood*, 1992, **80**, 505.
44 A. Muscella, N. Calabriso, S. A. DePascali, L. Urso, A. Ciccarese, F. P. Fanizzi, D. Migoni and S. Marsigliante, *Biochem. Pharmacol.*, 2007, **74**, 28.
45 J. W. M. Bulte, T. Douglas, B. Witwer, S.-C. Zhang, E. Strable, B. K. Lewis, H. Zywicke, B. Miller, P. van Gelderen, B. M. Moskowitz, I. D. Duncan and J. A. Frank, *Nat. Biotechnol.*, 2001, **19**, 1141.
46 G. R. Fulmer, A. J. M. Miller, N. H. Sherden, H. E. Gottlieb, A. Nudelman, B. M. Stoltz, J. E. Bercaw and K. I. Goldberg, *Organometallics*, 2010, **29**, 2176.

